04

Calculated and experimental determination of a laser spark length in the gas-jet targets

© A.N. Nechay, V.E. Guseva, A.A. Perekalov, N.I. Chkhalo

Institute of Physics of Microstructures, Russian Academy of Sciences, 607680 Nizhny Novgorod, Russia e-mail: valeriegus@ipmras.ru

Received October 31, 2024 Revised January 23, 2025 Accepted February 20, 2025

The paper presents results of investigation of sizes of the laser sparks that are generated when exciting the gas-jet targets based on argon, krypton and xenon by impulse radiation of the Nd:YAG-laser with the impulse duration of 4 ns and the impulse energy of $0.8\,\mathrm{J}$. The images of the laser plasma were obtained by means of an X-ray double-mirror microscope with five times magnification, that is based on the Schwarzschild lens, which operates at the wavelength of $11.25\,\mathrm{nm}$. The gas-jet targets were investigated at the nozzle inlet gas pressure of $2-10\,\mathrm{bar}$. The spark length values obtained from the experiment were compared with the theoretically calculated values.

Keywords: laser spark, extreme ultraviolet radiation, gas-jet targets.

DOI: 10.61011/TP.2025.07.61448.376-24

Introduction

Improvement of technological capabilities for producing multilayer X-ray mirrors (MXM) with increased reflectance has opened up capabilities in designing X-ray optical devices, including with use of chemical elements that are previously seldom used [1]. Thus, in particular, now there are the Mo/Be-based MXMs designed to effectively reflect at the wavelengths in the vicinity of 11 nm, which made it possible to use laser-plasma sources (LPS) of radiation at this wavelength within various laboratory X-ray optical installations, including lithographic ones [2]. As it is known, the wavelength of 11.25 nm corresponds to high-intense radiation of the xenon plasma [3,4] and is equivalent to a widely-used band of radiation of the tin plasma around 13.5 nm [5]. The tin plasma strongly pollutes the MXM during LPS operation, which is a significant drawback of this target [6]. When using xenon, it is possible to design a powerful "pure" radiation source that is operated at the wavelength of 11.25 nm and can be applied for industrial purposes, in particular, in nanolithography.

In order to design such powerful radiation sources for the lithographic applications, it is important to match the laser spark and the converging optics not only by operating wavelengths, but by a geometrical size of the laser spark area that radiates in the extreme ultraviolet (EUV) range. Thus, in a designed optical diagram of the test bench, a receiving X-ray optical element is a collector, whose surface is covered with MXM. The spark area, whence radiation is captured by the collector is $\sim 500\,\mu\text{m}$. It is planned to use the ultrasound xenon jets as targets for LPS. It is planned to excite the target by impulse laser systems with the average power density in a focus about $\sim 10^{12}\,\text{W/cm}^2$ and with a nano-second duration of the impulse. The sizes of the laser

sparks on the gas-jet targets have been already investigated by many authors [7–10]. But previously, the size of the laser spark area radiating at the perspective wavelength of 11.25 nm was not investigated systematically. Inter alia, we do not know a dependence of the laser spare size on parameters of the exciting laser radiation and the gas jet-target.

The present study has investigated the sizes of the laser sparks that are observed at the wavelength of 11.25 nm and formed at various parameters of the gas-jet targets and the exciting laser radiation. These measurements allowed determining the sizes of the laser spark generated in LPS, but they did not answer the question — at which parameters of the exciting laser radiation the spark length will be of the optimal value of $500 \,\mu m$. This question was solved by calculating the spark length in accordance with the theory described in the paper [11,12]. The values obtained as a result of the calculation were compared with those observed experimentally, and theory verification was followed by evaluating in a wide range the parameters of the exciting laser radiation and the gas-jet target. Based on the results of these calculations, requirements were made for the exciting laser system and the system of formation of the gas jet for their use in the various LPSes.

1. Experimental procedure

The experimental setup is shown in Fig. 1. The experiment was as follows: the impulse gas-jet target was formed with the gas leaving the conic ultrasound nozzle I into the vacuum chamber 2. By means of the lens 3, the laser radiation of the impulse Nd:YAG-laser 4 was focused on the target at the distance of 0.5 mm to a nozzle exit. An optical path of laser radiation to the target

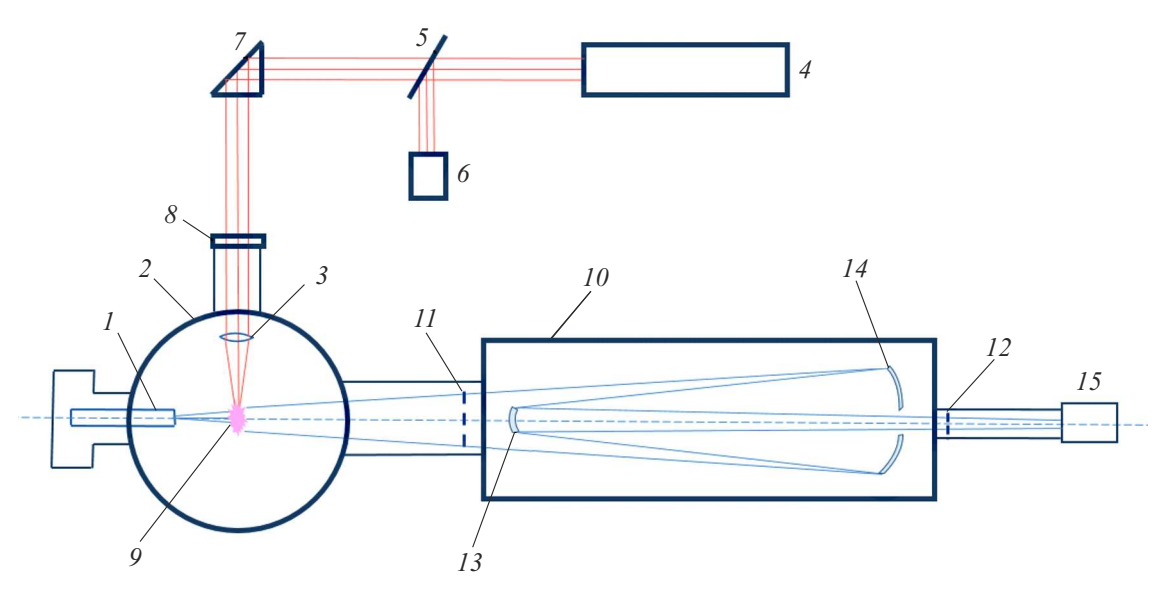


Figure 1. The experimental setup: *I* the ultrasound conical nozzle, *2*— the vacuum chamber, *3*— the focusing lens, *4*— the Nd:YAG-laser, *5*— the dividing plate, *6*— the power detector IMO-2, *7*— the prism, *8*— the input window, *9*— the laser spark, *10*— the X-ray microscope, *11*, *12*— the Zr/SiZr film filters, *13*— the convex MXM, *14*— the concave MXM, *15*— the matrix CMOS detector.

consists of the dividing plate 5 designed a small portion of radiation into the power detector IMO-2 6 and the prism 7 designed to direct radiation into the input window 8 of the vacuum chamber 2. In a focusing point, the laser-induced breakdown results in generation of highly-ionized plasma 9. The experimental setup is described in more detail in the paper [13].

The laser spark images were obtained by directing plasma radiation into an inlet of the double-mirror X-ray microscope with five times magnification 10 (Fig. 1), which was assembled in the Schwarzschild scheme. The EUV radiation of the laser plasma was highlighted by means of two freely-hanging filters based on Zr/SiZr 11 and 12 and arranged at an inlet and outlet of the microscope. The MXMs 13 and 14 used in the microscope effectively reflect radiation at the wavelength of 11.25 nm, wherein the reflectance is $\sim 67\%$. The microscope-built image is projected to a receiving matrix detector 15 of the GSENSE 2020 BSI grade, which operates on the CMOS technology. More details on the design and the characteristics of the microscope are given in the paper [14].

The experiment was done using the ultrasound conical nozzle with $d_{\rm cr}=500\,\mu{\rm m}$, of the length $L=5\,{\rm mm}$ and the flare half-angle $\alpha=4.5^{\circ}$, wherein the nozzle inlet pressure varied within the range 2–10 bar, the temperature was 300 K. Argon, krypton and xenon were used as the targets. With the used target parameters, the particle concentration in the zone of generation of the laser spark was about $1.5\cdot 10^{19}$ particles/cm³ [15]. The chamber vacuum was kept at the level of $10^{-2}\,{\rm Pa}$.

Excitation was done by the Nd:YAG-laser with the wavelength of $\lambda = 1064\,\mathrm{nm}$, the impulse duration of $\tau = 4\,\mathrm{ns}$, the pulse repetition rate of $10\,\mathrm{Hz}$ and the impulse energy of $0.8\,\mathrm{J}$. The optical system focused laser radiation with the

calculated diameter of $66 \,\mu\text{m}$. Thus, the power density of laser radiation within the focus area was $\sim 6 \cdot 10^{12} \, \text{W/cm}^2$.

The duration of shooting by the X-ray microscope was from several tenths of a second to several seconds and depended on intensity of spark radiation. Thus, when shooting the high-intense sparks of krypton and xenon, it was succeeded to obtain an image of the spark from one laser impulse. In order to obtain the image of the argon spark weakly radiating at the wavelength of 11.25 nm, a signal of several laser impulses was accumulated.

2. Experimental results

The experiment has resulted in obtaining the images of the laser sparks at the wavelength of $11.25 \, \mathrm{nm}$, which were produced with excitation of the different targets. Fig. 2 shows the images of the spark of argon (Fig. 2, a) and krypton (Fig. 2, b) at the nozzle inlet gas pressure of 8 bar and the spark of xenon at the pressure of 5 bar (Fig. 2, c). The laser beam is directed from bottom to top. The nozzle is located to the left of the spark. At the investigated wavelength, plasma radiation was chiefly formed by the ions Ar VII, Kr IX, Xe XI, respectively.

On Fig. 2, one can observe an asymmetry of the laser sparks in relation to a nozzle axis. The spark sizes were determined at intensity FWHM. The length-to-width ratio was 4 for argon, 10 for krypton and 3 for xenon. It can be seen that the spark formed at the gas-jet target of krypton is much narrower than the sparks formed at the gas-jet targets of argon and xenon.

Fig. 3 shows the dependence of the spark width on the pressure when exciting the targets of argon, krypton and

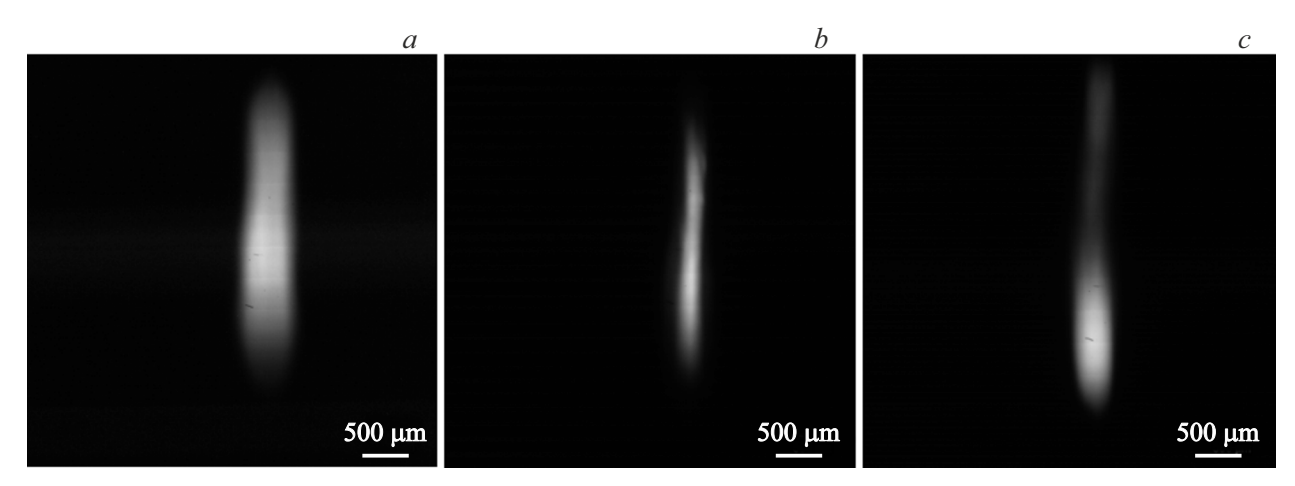


Figure 2. Images of the gas-jet targets based on argon (a), xenon (b) at the nozzle inlet gas pressure of 8 bar, xenon (c) at the nozzle inlet gas pressure of 5 bar.

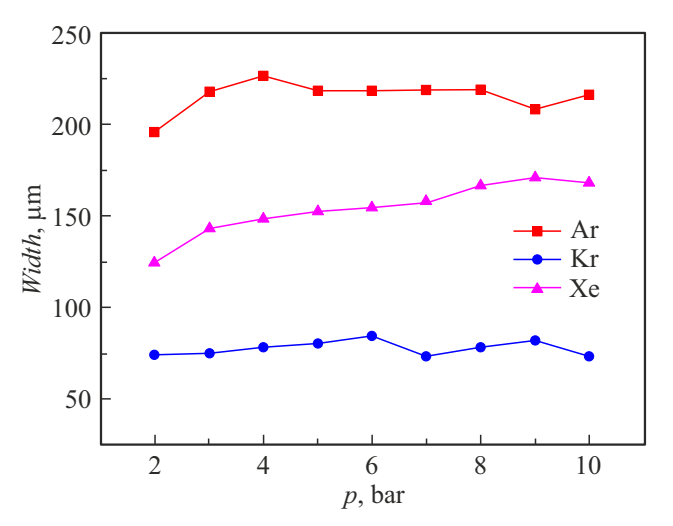


Figure 3. Dependence of the width of the sparks of argon, krypton and xenon on the nozzle inlet gas pressure.

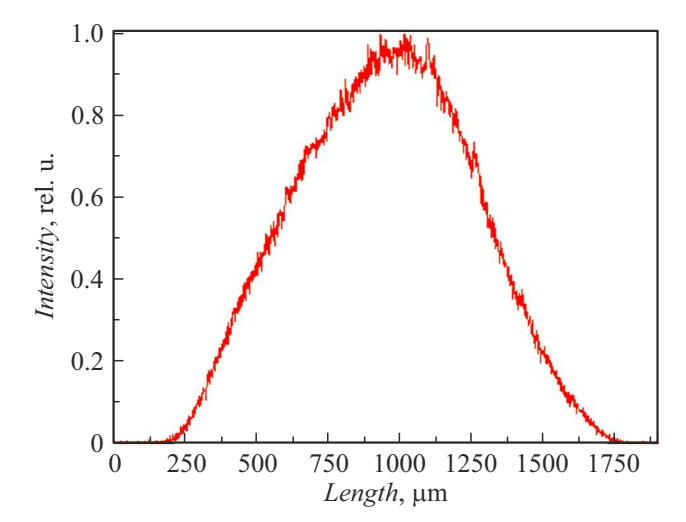


Figure 4. Distribution of intensity along the spark of argon at the nozzle inlet gas pressure of 5 bar.

xenon. The error of determination of the spark sizes due to resolution of the microscope is 3 pixels or $3.9 \mu m$.

It can bee seen on Fig. 3 that the spark width of the studied gas-jet targets weakly depends on the nozzle inlet gas pressure. Thus, the width of the spark of argon is $\sim 215\,\mu\text{m}$, so is that of krypton $\sim 75\,\mu\text{m}$, so is than of xenon $\sim 150\,\mu\text{m}$ at the gas pressures $2{-}10\,\text{bar}$.

With increase of the pressure from 2 to $10\,\mathrm{bar}$, the length of the spark of argon increases from 550 to $1030\,\mu\mathrm{m}$. Fig. 4 shows the distribution of intensity along the spark of argon at the nozzle inlet gas pressure of $5\,\mathrm{bar}$. The peak of radiation intensity is in the center of the jet. With variation of the nozzle inlet gas intensity, the form of the distribution of intensity along the length in the spark does not vary.

There is observed nonuniformity of distribution of EUV radiation along the spark It is most pronounced for the gasjet target based on xenon, which can be also seen on the image of Fig. 2, c. Fig. 5 shows the distributions of intensity

of radiation along the laser sparks of krypton (Fig. 5, a) and xenon (Fig. 5, b) at the various nozzle inlet gas pressures.

It can be seen on Fig. 5 with increase of the gas pressure, first intensity of the central part of the jet drops and then that of a far part along the laser beam drops. For the spark of xenon, this dependence is most pronounced (Fig. 5, lit b). Ultimately, for xenon at the pressures above 7 bar, there is only one peak left, which corresponds to a near part of the spark along the laser beam. These changes can be attributed to absorption of the observed EUV radiation in the gas of the gas-jet target. For xenon, absorption at the wavelength of 11.25 nm is the least among all the measured gases [16], which results in the most pronounced picture of distortion of the distribution of intensity along the spark. In case of krypton, at the studied gas pressures, influence of self-absorption does not change the values of the spark length, but only creates nonuniform distribution of intensity along it. Thus, it can be concluded that self-absorption in

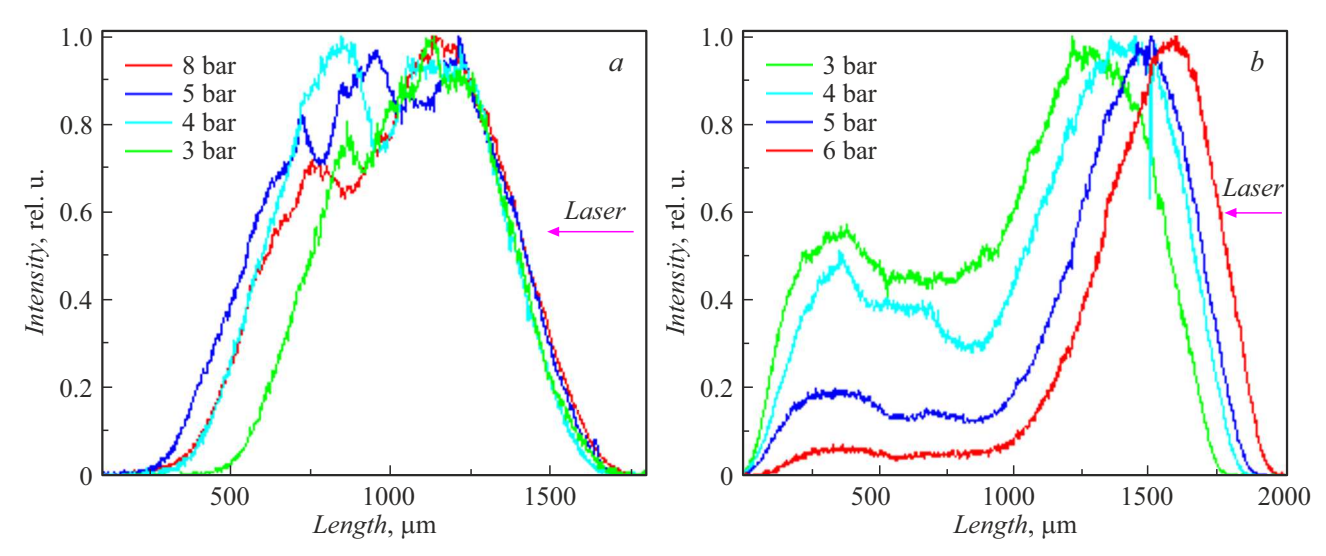


Figure 5. Distributions of intensity of radiation along the sparks of krypton (a) at the nozzle inlet gas pressures 3-8 bar and of xenon (b) at the nozzle inlet gas pressures 3-6 bar.

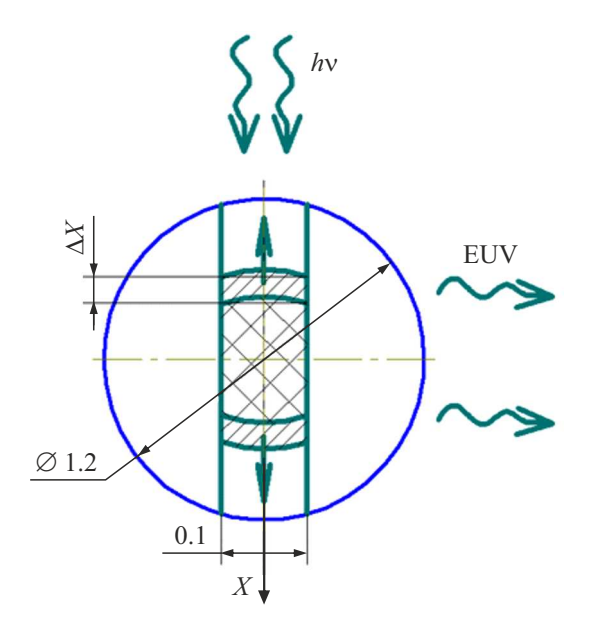


Figure 6. Diagram of formation of the laser spark.

the gas of the gas-jet target of krypton and xenon radically changes distribution of radiation intensity and a significant portion of EUV radiation is absorbed by the jet itself.

Fig. 6 shows a diagram of formation of the laser spark in accordance with the study [11,12]. The diagram shows a view from the conical nozzle that forms the gas target of the diameter of 1.2 mm. It also includes laser's incident radiation $h\nu$ that forms the laser spark of the diameter of $\sim 100\,\mu\mathrm{m}$ with two shock waves directed opposite to each other along the laser axis. Δx denotes the depth of an area of penetration of laser radiation into the target, which is the area of the densest plasma moving with a front of the laser detonation wave. It is clear from the diagram that nonuniform brightness of the source is due to the processes

of absorption of EUV radiation by the residual gas in a peripheral area of the target.

Based on the given diagram, it can be concluded that in order to reduce absorption of radiation in the gas-jet target this configuration requires a slit-like nozzle profile, not a circular one. The properly selected slit-like nozzle profile solves immediately several problems. First of all, the larger part of the target gas will be involved in formation of the laser spark. Consequently, a volume of the non-ionized target gas that actively absorbs EUV radiation will be reduced. Secondly, it will allow matching the laser spark and the distribution of the density of the gas-jet target. Thus, this profiling will make it possible to substantially reduce radiation absorption and increase intensity of the radiation source.

Performing numerical evaluations of the plasma parameters in the laser spark zone

The spark length was numerically determined using a model built on the study [11,12]. The model is based on a balance of energy that arrives from laser radiation and is spent for plasma heating and formation of detonation and shock waves.

Within the framework of this model, it is assumed that losses of plasma energy for radiation are small. Thus, all the absorbed energy of laser radiation is spent for ionization of the gas atoms, heating of the formed plasma, formation and propagation of the detonation wave along the laser beam and for energy losses through side walls of the detonation wave.

The model selected for performing the numerical evaluations of the basic parameters of the plasma in the laser spark zone includes the following number of the basic assumptions:

- 1) It is assumed that all the particles in the plasma, both ions and electrons, have the same temperature. The plasma temperature is quite high and strictly taking into account the distribution of the particles along the energies scarcely affects results of the evaluations. At the same time, taking into account the distribution of the particles along the energies complicates the calculation and takes simplicity from the model.
- 2) The gas-jet target is assumed to be unlimited with uniform distribution of the density. The performed measurements and the theoretical evaluations [15] show that a nucleus of the gas flow has a diameter of $\sim 1.2\,\mathrm{mm}$ and the particle concentration from the jet axis to the periphery varies by an order. The exact calculations of the particle concentration in such condensing jets are a quite difficult task and we have not performed them. Nevertheless, we consider it possible to use this approximation in the performed evaluations, taking into account smallness of the diameter of focusing of laser radiation.

Within the framework of the model, it is assumed that during formation of the laser spark the gas medium absorbs 100% of laser radiation entering it. Actually, absorption in the gas jets is 20%-80% of incident laser radiation depending on a gas grade and the density of the target particles. In order to take into account absorption coefficient of laser radiation absorbed by the target, the calculation process used the values of real absorption of the various gas-jet targets as measured by the authors in study [17]. The effective density of the laser radiation power was obtained by multiplying the calculated power density (under the condition of 100% absorption) by the absorption coefficient α that is determined experimentally.

The evaluations did not take into account distribution along the ionization degrees and the calculation formulas used the value of the maximum ion charge Z observed spectroscopically. Small sensitivity of the obtained results to variation of Z allows using this approximation.

The basics of this model are expressions for determining a velocity of propagation of the detonation wave and the density of the plasma internal energy [11,12]. The velocity of the detonation wave is determined as follows:

$$D = \left(2(\gamma^2 - 1)\frac{S_0 \delta}{\rho_0}\right)^{1/3}.$$
 (1)

The density of the plasma internal energy is determined as:

$$E = \frac{2^{2/3} \gamma}{(\gamma^2 - 1)^{\frac{1}{3}} (\gamma + 1)} \left(\frac{S_0 \delta}{\rho_0}\right)^{2/3}.$$
 (2)

Both the formulas have S_0 — the laser energy flux, ρ_0 — the gas density, γ — the adiabatic index for the plasma. The coefficient δ shows a portion of the absorbed laser energy spent for losses through the side surfaces of the detonation

wave and in this case it is determined as:

$$\delta = \frac{1}{1 + \frac{2a \cdot \Delta x}{rD}},\tag{3}$$

where a — the velocity of gas outflow through the side wall of the cylindrical detonation wave, r — the radius of the focus spot, Δx — the thickness of the absorbing layer.

The thickness of the absorbing layer is determined as a mean free path of a laser quantum:

$$\Delta x = l_w = \frac{T^{3/2} \cdot (h\omega)^2}{3.1 \cdot 10^{-31} \cdot Z^3 N^2 g},\tag{4}$$

where T — the plasma temperature, $h\omega$ — the energy of the laser radiation quantum, Z — the average charge of the plasma ions, N — the density of the gas atoms, g — the Gaunt factor determined as

$$g = 0.55 \ln \left[\frac{T2.4 \cdot 10^3}{Z^{\frac{4}{3}} N^{\frac{1}{3}}} \right].$$

Knowing the density of the internal energy of the plasma formed in the laser spark zone, it is possible to evaluate the plasma temperature by the following expression:

$$T = \frac{E \cdot M \cdot 1.66 \cdot 10^{-27} - I}{3/2(1+Z)k},\tag{5}$$

where M — the mass of the gas atom (the molecule for molecular gases) [amu], k — the Boltzmann constant, Z — the maximum charge of the plasma ions, I — the energy required for formation of the ions with the charge Z.

Within the framework of the used model, it is possible to evaluate the length of the radiating area by motion of the front of the detonation wave for the time of the laser impulse. Taking into account propagation of the wave front against and along the laser beam, we obtain the following formula for evaluation:

$$L \approx 2 \cdot D \cdot \tau + \Delta x,\tag{6}$$

where L — a typical size of the radiating area in a direction along the laser beam, Δx — the thickness of the absorbing layer.

In order to perform evaluations of the basic plasma parameters based on the selected model, it is necessary to establish numerical values of some parameters of the formulas such as: α , the density of the gas particles in the laser spark zone N, the maximum charge of the formed plasma cloud Z, I — the energy required for formation of the ion with the charge Z. These data were obtained as follows:

- 1) under the selected experimental conditions, the absorption coefficient of laser radiation by the gas-jet target was experimentally determined by the authors in the study [17];
- 2) the density of the gas particles in the laser spark zone was determined based on hydraulic- and gas-dynamic calculations given in the paper [15];

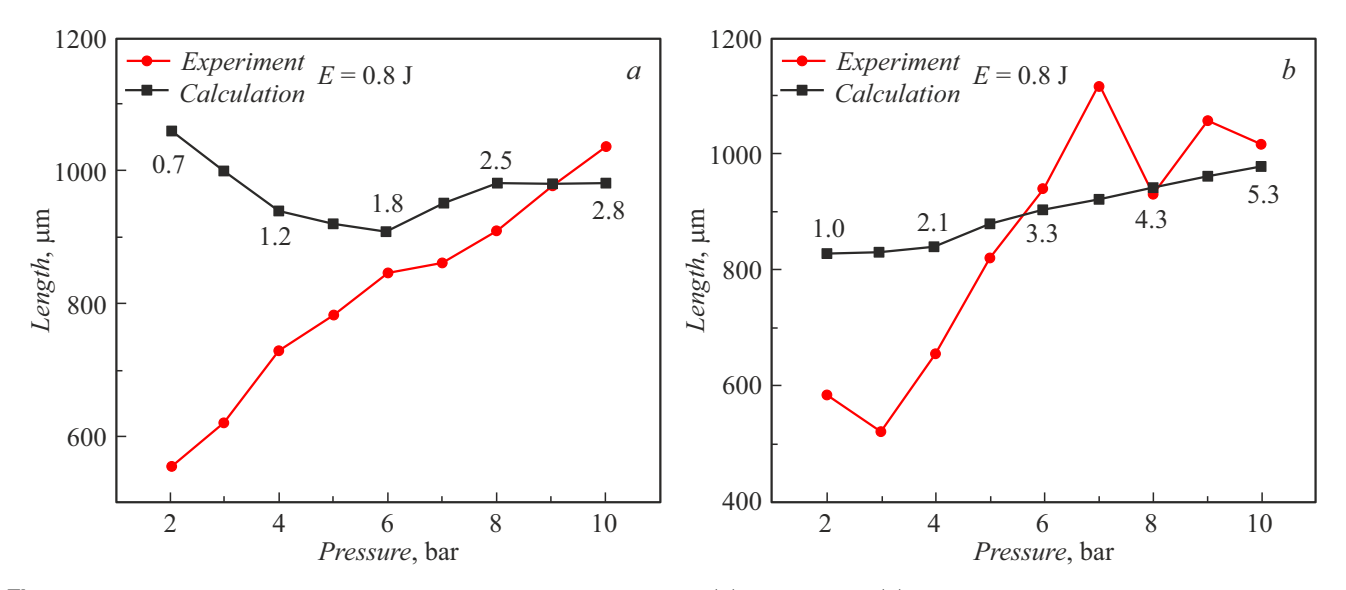


Figure 7. Calculated and experimental lengths of the sparks of argon (a) and krypton (b) depending on the nozzle inlet gas pressure.

3) the effective average charge of the plasma cloud Z was determined based on emission spectra previously obtained by the authors. The emission spectra were recorded in experimental conditions that corresponded to the calculation ones. The obtained spectra were published in earlier papers of the authors [18–20];

4) for the inert gases the parameter I was determined by the formula: $I = \sum i_n$, where i_n is a tabulated value of the ionization potential for the ion with the charge n. It was summed up to the maximum charge of the ions, whose emission lines are observed in the spectrum.

Thus, by means of the used model, it is possible to obtain estimates of the plasma temperature in the laser spark zone as well as the size of an area of discharge along the laser beam axis.

4. Comparison of the results

The present paper has compared the laser spark lengths that obtained experimentally and by calculations. The experimentally obtained spark length was shot by the profile of distribution of intensity along the spark at intensity FWHM. The error of determination of the spark sizes due to resolution of the microscope is 3 pixels or $3.9 \,\mu\text{m}$.

Fig. 7 shows the calculated and experimentally measured lengths of the sparks of argon (Fig. 7, a) and krypton (Fig. 7, b) depending on the nozzle inlet gas pressure. In the calculation and during the experiment, the energy of the laser impulse was a constant value being 0.8 J. The digits denote the calculation values of the temperature in 10^6 K, which correspond to points at the various gas pressures.

It is clear from Fig. 7, a that with increase of the gas pressure the experimentally measured length of the spark of argon increases almost linearly. But the calculated dependence is different — with increase of the gas pressure

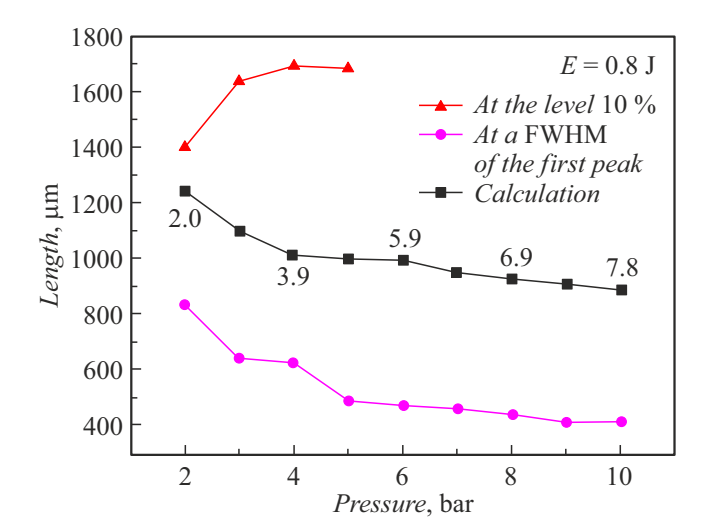


Figure 8. Calculated and experimental lengths of the sparks of xenon depending on the nozzle inlet gas pressure.

from 2 to 6 bar the length of the spark decreases, and then with the pressure above 6 bar it slightly increases.

It is clear from Fig. 7, b that the experimentally measured length of the spark grows with increase of the pressure to 6 bar, and after that the growth is nearly stopped. The calculated dependence demonstrates a smooth slow growth with increase of the gas pressure.

During the measurements by the EUV microscope, radiation at the wavelength of 11.25 nm was recorded, which corresponds to radiation of the ions Ar VII and Kr IX, wherein the energy of their formation in a temperature scale corresponds to the temperature 1.7 and $2.7 \cdot 10^6$ K, respectively. It can be seen on Fig. 7 that there is a discrepancy of the experiments with the theory, which decreases with increase of the nozzle inlet gas pressure.

This phenomenon can be explained by the fact that at the low nozzle inlet gas pressures a low-temperature plasma is formed, wherein only the central zone of the forming laser spark is highlighted at the wavelength of $11.25\,\mathrm{nm}$. The match between the experiments and the theoretical calculations is satisfactory at the pressures $6-10\,\mathrm{bar}$ for the spark of argon and $4-10\,\mathrm{bar}$ for the spark of krypton. At the high densities of the target, the plasma is more strongly heated and its temperature is sufficient for significant emission of radiation at the wavelength of $11.25\,\mathrm{nm}$.

Besides, with this consideration it is clear why the plasma of krypton has a higher length-to-width ratio — only the axial part of the laser spark is highlighted at the operating wavelength of the microscope.

Fig. 8 shows the calculated and experimentally measured lengths of the sparks of xenon depending on the nozzle inlet gas pressure. Due to absorption of radiation by the gas of the gas-jet target (Fig. 5, b), there are observed strong distortions of the form of the recorded laser spark. So, for fuller description of a picture of the experimental data it includes the length of the laser spark at the level of 10% of the peak height and at the FWHM of the first peak. With increase of the pressure, the length of the laser spark at the level of 10% of the peak increases at the pressures up to 5 bar. At the pressure of 6 bar, the observed length of the spark sharply declines as a result of strong self-absorption, and therefore only the length of the first peak is presented below. The length of the laser spark at the FWHM of the first peak decreases with increase of the nozzle inlet gas pressure. The calculated dependence demonstrates smooth reduction of the length of the spark with increase of the gas pressure. The digits denote the calculation values of the temperature in 10⁶ K, which correspond to points at the various gas pressures. During the experiment, the energy of the laser impulse was a constant value being 0.8 J.

During the measurements by the EUV microscope, radiation at the wavelength of 11.25 nm was recorded, which corresponds to the ion Xe XI, wherein the energy

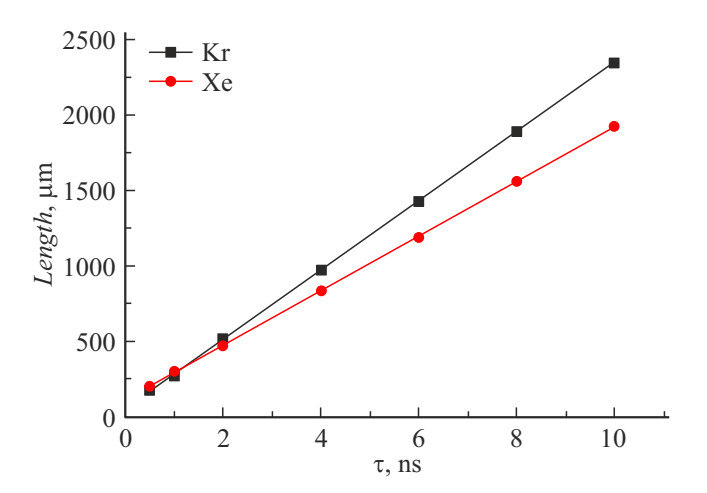


Figure 9. Calculated dependence of the lengths of the sparks of argon and krypton on the duration of the laser impulse.

of its formation in a temperature scale corresponds to the temperature of $2.7 \cdot 10^6 \, \mathrm{K}$. It can be presumed that the theoretical calculations adequately describe the length of the spark of xenon at the nozzle inlet gas pressure above 4 bar and the calculated temperature of $3.9 \cdot 10^6 \, \mathrm{K}$. In this case, the length of the spark of xenon without taking into account self-absorption will be close to 1 mm. During this research, an extremely important role belongs to absorption of EUV radiation by xenon in the peripheral areas of the jet. Thus, for correct comparison of the experiments with the calculations, it is necessary to make measurements on slit-like nozzles, for which self-absorption will be reduced.

To match the length of the laser spark with a field of view of the collector, it is necessary that the spark size would not exceed $500\,\mu\text{m}$. The length of the spark can be reduced by decreasing the duration of the laser impulse. This dependence can be determined based on the used model. At this, the calculations included variation of the energy of the laser impulse as well, so as to keep the power density of the exciting laser radiation unchanged. The calculated nozzle inlet gas pressure was assumed to be 10 bar. The calculation results are shown in Fig. 9.

It can be seen on Fig. 9 that the length of the spark linearly increases with increase of the duration of the impulse with the unchanged power density. At the same time, the plasma temperature in the area of discharge is still a constant. Returning to the formula (6), the length of the spark increases only due to the longer time of propagation with the unchanged velocity of and the unchanged depth of penetration of laser radiation that depend on the power density. In order to obtain the spark length required for the designed laboratory lithograph, the duration of the exciting laser impulse shall be 2 ns while maintaining the power density in the focus at about $10^{12} \, \text{W/cm}^2$.

Conclusion

The X-ray microscope with the operating wavelength of 11.25 nm has been used to obtain the images of the laser sparks formed by excitation of the gas-jet targets of argon, krypton and xenon with the impulse laser radiation.

It included investigation of the sizes of the sparks produced in the laser-plasma radiation sources with the gas-jet targets. The width of the sparks was $\sim 215\,\mu\mathrm{m}$ for the target of argon, $\sim 75\,\mu\mathrm{m}$ for the target of krypton and $\sim 150\,\mu\mathrm{m}$ for the target of xenon and it is almost independent of the nozzle inlet gas pressure. The length of the sparks measured at FWHM of radiation intensity was from 550 to $1030\,\mu\mathrm{m}$ for the target of argon, from 230 to $980\,\mu\mathrm{m}$ for the target of krypton and from 830 to $415\,\mu\mathrm{m}$ for the target of xenon at the nozzle inlet gas pressures from 2 to 10 bar. The study has also included the theoretical evaluations of the spark lengths. The results of the experiment and theoretical calculation match with the nozzle inlet gas pressures above 6 bar.

It is found that with using the xenon jets as the target self-absorption of the EUV radiation substantially affects the distribution of intensity along the spark axis. To overcome this, it is proposed to use a special slit-like nozzle profile. This profiling will make it possible to substantially reduce radiation absorption in the gas jet and increase intensity of the radiation source.

Besides, it has calculated the dependence of the spark lengths when exciting the targets of krypton and xenon on the duration of the laser impulse while maintaining the power density of the exciting laser radiation. It is shown that in order to obtain the laser spark length that is optimal for the lithographic application, it is necessary to use the laser systems with the short impulse duration of $\sim 2\,\mathrm{ns}$.

Funding

The experimental study was carried out under the state assignment of the Institute of Applied Physics of the Russian Academy of Sciences (RAS IAP), the subject of the state assignment: FFUF-2025-0006. The theoretical part was supported financially by the Ministry of Science and Higher Education of the Russian Federation (the agreement N 075-15-2021-1361).

Conflict of interest

The authors declare that they have no conflict of interest.

References

- M.V. Svechnikov, N.I. Chkhalo, S.A. Gusev, A.N. Nechay, D.E. Pariev, A.E. Pestov, V.N. Polkovnikov, D.A. Tatarskiy, N.N. Salashchenko, F. Schäfers, M.G. Sertsu, A. Sokolov, Y.A. Vainer, M.V. Zorina. Opt. Express, 26 (26), 33718 (2018).
- [2] N.I. Chkhalo, N.N. Salashchenko. AIP Adv., 3 (8), (2013).
- [3] V.E. Guseva, A.N. Nechay, A.A. Perekalov, N.N. Salashchenko, N.I. Chkhalo. Appl. Phys. B, 129 (10), 155 (2023).
- [4] S.G. Kalmykov, P.S. Butorin, M.E. Sasin. J. Appl. Phys., 126 (10), (2019).
- [5] I. Fomenkov, D. Brandt, A. Ershov, A. Schafgans, Y. Tao, G. Vaschenko, S. Rokitski, M. Kats, M. Vargas, M. Purvis, R. Rafac, B. La Fontaine, S. De Dea, A. LaForge, J. Stewart, S. Chang, M. Graham, D. Riggs, T. Taylor, M. Abraham, D. Brown. Adv. Opt. Technol., 6 (3-4), 173 (2017).
- [6] G. Niimi, Y. Ueno, K. Nishigori. In Emerging Lithographic Technologies VII. SPIE, 5037, 370 (2003).
- [7] J. Holburg, M. Müller, K. Mann, S. Wieneke. J. Vacuum Sci. Technol. A, 37 (3), (2019).
- [8] V.E.E. Levashov, K.N. Mednikov, A.S. Pirozhkov, E.N. Ragozin. Quant. Electron., 36 (6), 549 (2006).
- [9] G.D. Kubiak, L.J. Bernardez II, K.D. Krenz. In Emerging Lithographic Technologies II. SPIE, **3331**, 81, (1998).
- [10] S. Kranzusch, K. Mann. Opt. Commun., **200** (1–6), 223 (2001).

- [11] B. Zel'dovich, Yu. Raizer, Fizika udarnykh voln i vysokotemperaturnykh gidrodinamicheskikh yavlenii (Nauka, Glav. red. Fizmatlit, M., 1974) (in Russian).
- [12] Yu.P. Raizer. Lazernaya iskra i rasprostraneniye razryadov (Nauka, M., 1974) (in Russian).
- [13] A.N. Nechay, A.A. Perekalov, N.I. Chkhalo, N.N. Salashchenko, I.G. Zabrodin, I.A. Kas'kov, A.E. Pestov. Poverkhnost'. Rentgenovskie, sinkhrotronnye i neitronnye issledovaniya, (9), 83 (2019) (in Russian).
- [14] A.A. Perekalov, V.E. Guseva, I.V. Malyshev, A.N. Nechay, A.E. Pestov, D.G. Reunov, R.M. Smertin, M.N. Toropov, N.N. Tsybin, N.I. Chkhalo. Rev. Sci. Instruments. Accepted (2023).
- [15] M.A. Korepanov, M.R. Koroleva, E.A. Mitrukova. J. Phys.: Conf. Ser., 2057 (1), 012016 (2021).
- [16] R. de Bruijn, K. Koshelev, G. Kooijman, E.S. Toma, F. Bijk-erk. J. Quant. Spectr. Radiative Transfer, 81 (1-4), 97 (2003).
- [17] V.E. Guseva, I.G. Zabrodin, A.N. Nechay, A.A. Perekalov, N.I. Chkhalo. ZhTF. 95 (7), (2025) (in Russian).
- [18] A.N. Nechay, A.A. Perekalov, N. N. Salashchenko, N.I. Chkhalo. Opt. i spektr., 129 (2), 146 (2021) (in Russian).
- [19] A.N. Nechay, A.A. Perekalov, N. N. Salashchenko, N.I. Chkhalo. Opt. i spektr., 129 (3), 266 (2021) (in Russian).
- [20] A.N. Nechay, A.A. Perekalov, N.I. Chkhalo, N. N. Salashchenko. Opt. i spektr., 129 (6), 755 (2021) (in Russian).

Translated by M.Shevelev